Study of the Permeation Flowrate of an Innovative Way to Store Hydrogen in Vehicles

Gustavo Pinto [1,2,*], Joaquim Monteiro [1,2], Andresa Baptista [1,2], Leonardo Ribeiro [1,2] and José Leite [1]

1   ISEP—School of Engineering, Polytechnic of Porto, 4200-072 Porto, Portugal; jfmo@isep.ipp.pt (J.M.);
    absa@isep.ipp.pt (A.B.); lsr@isep.ipp.pt (L.R.); 1150343@isep.ipp.pt (J.L.)
2   INEGI—Instituto de Ciência e Inovação em Engenharia Mecânica e Engenharia Industrial,
    4200-465 Porto, Portugal
*   Correspondence: gflp@isep.ipp.pt; Tel.: +351-228-340-500

Abstract: With the global warming of the planet, new forms of energy are being sought as an alternative to fossil fuels. Currently, hydrogen (H_2) is seen as a strong alternative for fueling vehicles. However, the major challenge in the use of H_2 arises from its physical properties. An earlier study was conducted on the storage of H_2, used as fuel in road vehicles powered by spark ignition engines or stacks of fuel cells stored under high pressure inside small spheres randomly packed in an envelope tank. Additionally, the study evaluated the performance of this new storage system and compared it with other storage systems already applied by automakers in their vehicles. The current study aims to evaluate the H_2 leaks from the same storage system, when inserted in any road vehicle parked in conventional garages, and to show the compliance of these leaks with European Standards, provided that an appropriate choice of materials is made. The system's compliance with safety standards was proved. Regarding the materials of each component of the storage system, the best option from the pool of materials chosen consists of aluminum for the liner of the spheres and the envelope tank, CFEP for the structural layer of the spheres, and Si for the microchip.

Keywords: hydrogen; permeation; safety; energy storage system; green energy; vehicle propulsion

1. Introduction

Almost 87% of human CO_2 emissions worldwide are caused by fossil fuel use [1]. In the last few years, there has been great concern from the governments of several countries to provide a global and effective response to halt the increase of the global average temperature of the Earth and tackle the challenges related to climate change [2].

This effort was translated into the Paris Agreement, which aims to decarbonize world economies [3]. However, the targets for reducing carbon emissions imposed by the Paris Agreement have been questioned, concerning its suitability with the reduction of energy poverty [4]. Thus, in the search for decarbonization, it is expected that hydrogen (H_2) will soon be considered an important energy vector, either for propulsion or for energy storage [2,5–7].

The sustainable future involves the use of smart energy solutions and, consequently, the interests of many authors have been aroused to this topic [4,8,9]. Dincer and Acar [8] highlight that smart energy solutions are not possible without solutions that use hydrogen. They also reinforce the importance of sustainable methods of hydrogen production, which are still challenging, for a carbon-free economy. They concluded that requirements such as (i) energy conservation, (ii) the use of renewable energy, (iii) integration of clean energy, (iv) increase of valuable products from the same resources, (v) more efficient storage of energy carriers and chemicals, and (vi) the use of smart grids and control in renewable energy are the minimum and necessary requirements for a transition to a smart solution based on H_2, given a sustainable future [8].

The use of H_2 as fuel is still in its embryonic stage and it is necessary to create conditions to support its distribution and storage, including infrastructure (refueling stations), that are safe and fast to meet the necessary conditions for the common use of hydrogen [10,11].

The environmental impact of using H_2 as fuel in vehicles has been studied by comparing hydrogen-propelled vehicles with electric vehicles charged with electricity obtained from renewable sources [12,13]. Some studies include the production of H_2 from renewable energy (sun, wind, tides, among others), also known as green energy. These investigations show the great interest in H_2 storage since it is economically feasible to store large amounts of energy, in the form of H_2, according to the seasonal rhythms of the availability of green energy [14–17]. Indeed, to reduce the impact of obtaining H_2, the surplus production of renewable energies should be used to obtain H_2, which would be stored before being used [18]. Tarkowski [19] studied the feasibility of underground storage in different contexts, such as deep aquifers, depleted oil fields, salt caves, and depleted gas fields, and concluded that the differences between underground hydrogen storage and natural gas storage are not significant.

A competitive and ecological alternative to battery-powered electric vehicles is the use of vehicles propelled by stacks of fuel cells, which may become an economic reality. H_2 for fuel cells could achieve large-scale use in vehicles as renewable energy becomes more widespread [20–22]. One of the main challenges for this is a quick and safe supply of H_2 [23].

In line with the growing interest in the use of H_2 for vehicle propulsion, the concern for storing this fuel in vehicles has also grown. Thus, Fonseca et al. [18] state that almost 70% of publications on the H_2 topic focus on hydrogen storage. It should be noted that storage of hydrogen entails safety questions, and it should not compromise the useful space for passengers or cargo.

It is possible to distinguish two distinct ways of storing hydrogen [6]. The first one consists of storing it as (i) compressed gas (CGH_2), (ii) cryogenic liquid, (iii) adsorbed on carbon nanofibers, or (iv) adsorbed on metal or reversible metal hydride [6,24]. In a second way, H_2 is stored in the molecules of ammonia (NH_3) or methanol (CH_3OH), among others. The most widespread storage method for H_2, either in stationary applications or in vehicles, uses man-made pressurized containers, namely cylinders of various sizes; for stationary facilities, underground caves can be used. Larminie et al. [24] presented some advantages regarding the storage of H_2, taking CGH_2 as an example, namely the unlimited storage time, its simplicity, and no requirement of purity in H_2.

The current study is a follow-up to a previous paper [25], whose purpose was to assess a new system, proposed by Stenmark [26], to store H_2 in conventional vehicles. The investigation focused on the high-pressure H_2 storage system inside small spheres stowed randomly in a container, hereafter named the envelope tank, with dimensions similar to a conventional fuel tank used in current vehicles. Thus, such assessment was made based on: (i) the energy stored by weight of the system (GED), (ii) the energy stored by the volume of the system (VED), (iii) the leakage of H_2 from the system, through the comparison with other methods of H_2 storage and, finally, (iv) the compliance with current safety standards was checked. In the referred previous study, the main characteristics of the complete storage system (envelope tank and spheres) were studied, using spheres of 10 different materials, with an internal diameter of 10 to 70 mm. The following parameters were also considered: a packing factor between 52 and 74%, a safety factor of 1.41, a tank with an internal volume of 0.122 m^3, and two types of microchip material were considered. From the study, the best combination of materials for the sphere composition was a structural layer in CFEP, a liner in aluminum, and a microchip in silicon. With this combination, the system achieved a VED between 0.61 and 0.87 kWh/L and a GED between 6.62 and 7.22 kWh/kg.

Figure 1 shows a comparison of the GED and VED of several fuels, including the spheres storage system of Stenmark [26], whereby it is possible to confirm the clear advantage of the new storage method, taken as new fuel, concerning the other systems.
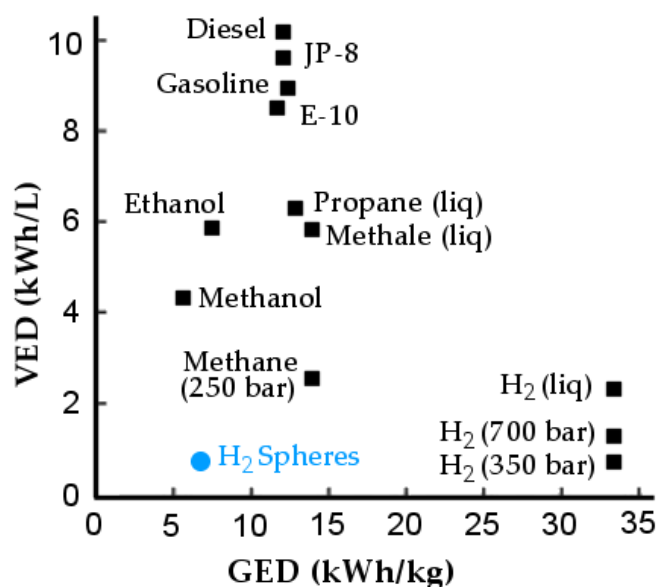

Figure 1. Comparison between GED and VED for the new storage system, taken as a new fuel, and other fuels, adapted by the U.S. Department of Energy.

H_2 materials for storage containers must be chosen carefully, always considering the limitations and requirements of the European Regulations [27]. An important parameter is the size of the H_2 molecule since it is the smallest, which results in its high average speed. Thus, the permeation of H_2 through the walls of a container cannot be neglected. Care must also be taken, for example, if the container is metallic because small H_2 bubbles will appear and create small cracks in the walls of the container. In the case that the container is made of metallic alloys with carbon, such as steel, it is likely there will be a reaction between the H_2 and carbon, resulting in CH_4 bubbles. As a result of this reaction, the walls will crack—a phenomenon known as H_2 embrittlement. According to the authors [24,28,29], a way to avoid this phenomenon is the addition of molybdenum and chromium to steel.

Another important point to consider is the danger associated with H_2 leakage, mostly for a container at very high pressure. Upon leakage, the H_2 self-ignites in a flammability range of 4 to 77% (*v/v*), and an invisible flame is generated. The solutions found to minimize the associated risks are the introduction of rupture discs, relief valves, and flame traps installed in the tanks.

According to Adams et al. [30], it seems that the H_2 flowing by permeation (typically low flowrates) from a container into a compartment such as a garage, spreads almost evenly across the available space, without noticeable stratification, in spite of its much lower density than the density of the air. The authors calculated the maximum allowable permeation flowrate from the H_2-polymer-containers for typical cars and city buses; this calculation took into account the initial mass/pressure of H_2 within the containers, the dimensions (ultimately the volume) of the compartment where the car is parked, the age of the polymer (which affects the permeability of the container), the temperature the polymer is subjected to (which also affects the permeability of the container), and the air change flowrate of the compartment, allowing a maximum percentage of H_2 in the compartment of 1% (*v/v*). For safety reasons, this is well below the lower flammability limit of H_2 in the air.

Crowl et al. [31] conducted a study where they distinguished the dangers and risks regarding the use of H_2. They defined the hazards linked to flammability, and the risks linked to the combination of the probability of an accident and the consequences of the

accident. This question demands considering the minimum ignition energy of H_2, which is very low when compared to the homologous value for other gases, whereby it follows that the combustion of H_2 is easily activated. Another characteristic of H_2 to consider is its high range of flammability. It is necessary to limit the amount of H_2 in confined spaces. The high diffusivity of H_2 facilitates the aeration of spaces, and its low molecular weight promotes its upward dispersion.

The main purposes of the present study are, firstly, to assess the flowrate due to permeation of H_2 for a new storage system (envelope tank and spheres) when it is used in any road vehicle parked in a conventional garage, and, secondly, to show the compliance of these leaks with the European Regulations [27], provided a suitable choice of materials is made.

2. Methodology for Assessing the Performance of the System

As already stated, the current study addresses an innovative way of storing H_2 in common vehicles. The methodology followed to evaluate the performance of this storage system is described in Table 1 as a chain of steps.

Table 1. Steps summary.

Step 1	Storage system description
Step 2	Time variation of pressure and mass in spheres and in tank
Step 3	Materials selection for the sphere, tank, and the values of permeation
Step 4	Regulation that must be complied
Step 5	Aim of calculations
Step 6	The packing factor (PF)

2.1. Storage System Description: Step 1

The system consists of a set of small spheres randomly packed inside an envelope tank with any shape. In Figure 2, an example can be seen, with a "parallelepiped" envelope tank in the trunk of the vehicle. H_2 is inside the spheres at high pressure, say 700 bar, and at room temperature. All spheres have an embedded parallelepiped microchip, with dimensions of $0.5 \times 0.5 \times 2.5$ mm^3. Either the refilling of the empty spheres with H_2 or the release of H_2 from filled spheres are controlled through the microchip. If the internal pressure of the tank is below a chosen pressure threshold, say 5 bar, the spheres do not release H_2 into the tank, but if that pressure is above the said threshold, then the spheres release H_2 into the tank; in this study, the maximum operating pressure of H_2 in the tank was considered as 20 bar. The propeller, either a reciprocating spark-ignition engine or a stack of fuel cells, is fed by the tank.
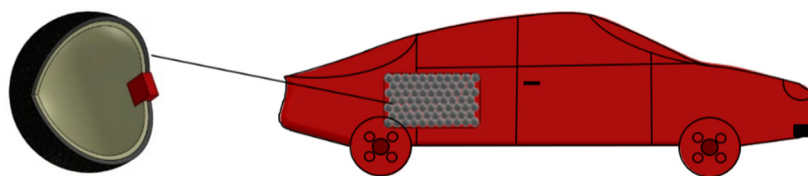
Figure 2. New H_2 storage system in a common car.

2.2. Time Variation of Pressure and Mass in Spheres and in Tan: Step 2

The permeation flow of H_2 from the storage system occurs because of the permeability of the micro-spheres and of the envelope tank. It is important, for safety reasons, to determine if the flowrate of H_2, due to permeation during a prolonged stop of the vehicle, compromises the safety of the garage where the vehicle is parked. Thus, it is necessary to know the pressure, mass of H_2, permeation flowrate of H_2, and concentration of H_2 over time, for the micro-spheres, the envelope tank, and the garage.

This emptying of the storage system (spheres and envelope tank) is time-dependent. Yet, the calculations performed, and described below, assume a succession of time intervals,

as small as required for the sake of accuracy, within which it is plausible to assume a steady state.

A description of the procedure used follows:

1. Mass of H_2 within a sphere is given by (1),

$$M_{H_2-sph} = \frac{P_{sph} \cdot V_{in\ sph}}{Z \cdot R_{H_2} \cdot T_{H_2}} \tag{1}$$

2. Concentration of H_2 within a sphere is given by (2) since the mole fraction $xH_2 = 1$ within the spheres.

$$[H_2]_{sph} = \frac{P_{sph}}{Z \cdot R_u \cdot T_{H_2}} \tag{2}$$

3. Concentration of H_2 within the envelope tank is given by (3) since the mole fraction $x_{H2} = 1$ within the envelope tank.

$$[H_2]_{tank} = \frac{P_{tank}}{Z \cdot R_u \cdot T_{H_2}} \tag{3}$$

4. A part of the inner volume of the envelope tank is occupied by spheres, whose volume is given by (4),

$$V_{ts} = PF \times V_{int\ tank.} \tag{4}$$

5. Mass of H_2 contained in the part of the envelope tank free of spheres is given by (5),

$$M_{H_2-tank} = \frac{P_{tank} \cdot (1-PF) V_{int\ tank}}{Z \cdot R_{H_2} \cdot T_{H_2}}. \tag{5}$$

6. The permeation coefficient, Φ, of H_2 was taken from tables [32]; its value is expressed either by mole/m/s/MPa, or mole/m/s/MPa$^{1/2}$, or mole/m^2/s/MPa$^{1/2}$.

7. The solubility, S, of H_2 was calculated as the quotient of H_2 by the partial pressure of H_2 if the permeation was expressed as mole/m/s/MPa, or as the quotient of H_2 by the root of the partial pressure of H_2, if the permeation was either expressed as mole/m/s/MPa$^{1/2}$ or mole/m^2/s/MPa$^{1/2}$. The partial pressure of H_2 within the spheres equals the total pressure within the spheres; the partial pressure of H_2 within the envelope tank equals the total pressure within it; the H_2 in the atmosphere was considered zero.

8. The diffusivity, D, of H_2 across each layer of the spheres and across the envelope tank was calculated with (6). In the case of the permeability being expressed in mole/m^2/s/MPa$^{1/2}$, which was the case with Si for the microchip, to obtain the diffusivity in m^2/s it was necessary to multiply the permeability by the thickness of the layer.

$$\Phi = DS. \tag{6}$$

9. Each micro-sphere is made of two concentric spheres, or layers, of different materials, and a parallelepipedal microchip embedded in both spheres; moreover, the outer diameter of the inner sphere equals the inner diameter of the outer sphere. The inner layer, named liner, is mostly intended to provide the necessary resistance to H_2 permeation and the outer layer, named structural, is mostly intended to provide structural strength. The permeation flow of H_2 from the micro-spheres must not be confounded with the intentional flow of H_2 from the spheres, controlled by the microchip, to fuel the propeller (engine or fuel cells). The former occurs in three different ways: by permeation through the spheric layers, by permeation through the microchip, and by the interface between the microchip and the sphere (which is unwanted). This latter flow is leakage and should be as small as possible; since it depends on the quality of the manufacture of the micro-spheres, it is human-controlled

and will be neglected. Thus, the overall diffusivity for a micro-sphere is given by (7): it was calculated considering the flow across the series of the composite wall of two concentric spheres (liner and structural) in parallel with the flow across the microchip. As referred, $r_{o\ liner} = r_{i\ strut}$.

$$D_{Total} = \left(\frac{1}{r_{i\ liner}} - \frac{1}{r_{o\ stru}} \right) \left[\frac{D_{microchip} A_{microchip}}{4\pi t_{microchip}} + \frac{1}{\frac{1}{D_{liner}}\left(\frac{1}{r_{i\ liner}} - \frac{1}{r_{o\ liner}} \right) + \frac{1}{D_{stru}}\left(\frac{1}{r_{i\ stru}} - \frac{1}{r_{o\ stru}} \right)} \right], \quad (7)$$

10. Total resistance to the diffusion of H_2 through a micro-sphere was calculated with Equation (8).

$$R_{micro-sphere} = \frac{1}{4\pi D_{Total}} \left(\frac{1}{r_{i\ liner}} - \frac{1}{r_{o\ stru}} \right) \quad (8)$$

11. Mole flowrate of H_2 through a micro-sphere was calculated by (9); the concentrations of H_2 were considered at the inner face of the liner, and at the outer face of the structural layer.

$$\dot{n}_{H_2\ micro-sphere} = \frac{[H_2]_{i\ liner} - [H_2]_{o\ stru}}{R_{micro-sphere}} \quad (9)$$

12. Masses of H_2 within a micro-sphere at the instant t, and at the instant t-Δt are related through (10).

$$M_{H_2\ micro-sphere}(t) = M_{H_2\ micro-sphere}(t - \Delta t) - \dot{n}_{H_2\ micro-sphere}(t) MW_{H_2} \Delta t \quad (10)$$

13. Concentration of H_2 within the envelope tank was obtained through (3) but was considered zero outside it, at the surrounding atmosphere.

14. Solubilities of H_2 at the inner and outer surface of the envelope tank were calculated according to point 7. The diffusivity of H_2 through the envelope tank was calculated according to Equation (6).

15. It was assumed a cylindrical enveloped tank, so the total resistance to the diffusion of H_2 through the envelope tank was calculated with Equation (11).

$$R_{tank} = \frac{ln\left(\frac{r_{t\ o}}{r_{t\ i}} \right)}{2\pi L D_{tank}} \quad (11)$$

16. Mole flowrate of H_2 through the envelope tank to the atmosphere was calculated by (12), where the concentrations of H_2 were considered at the inner face of the envelope tank and at the outer face of the envelope tank; the value of the H_2 concentration in the envelope tank was assumed to be zero.

$$\dot{n}_{H_2\ tank} = \frac{[H_2]_{i\ tank} - [H_2]_{o\ tank}}{R_{tank}}. \quad (12)$$

17. Masses of H_2 within the part of the envelope tank free of micro-spheres at the instant *t*, and at the instant *t-Δt* are related through Equation (13).

$$M_{H_2\ tank}(t) = M_{H_2\ tank}(t - \Delta t) + MW_{H_2} \Delta t \left[N_{micro-spheres} \dot{n}_{H_2\ micro-sphere}(t) - \dot{n}_{H_2\ tank} \right] \quad (13)$$

18. At any instant t, the pressure within the micro-spheres or in the part of the envelope tank free of micro-spheres was calculated with the equation of perfect gases. The same was done regarding the H_2 concentrations.

RH_2 is the ideal gas H_2 constant, taken as 4124 Jkg^{-1}K^{-1}; Ru is the universal constant of perfect gases; MWH$_2$ is the molecular weight of H_2 considered as 2.016 kg kmol^{-1}; TH$_2$ is the temperature of H_2, assumed as 293.15 K; and Z is the compressibility factor of H_2 at 700 daNcm^{-2} and 293.15 K, taken as 1.46 [33].

2.3. Materials Selection for the Sphere, Tank, and the Values of Permeation: Step 3

The studied materials, as well as their most relevant properties for the present study, are shown in Table 2. The silicon (Si), present in Table 2, was considered only for the microchip.

Table 2. Materials properties for the sphere and microchip.

Material	Φ		ρ (kgm^{-3})	σ_{yield} (MPa)	σ_{ult} (MPa)	References
Al 5050-H38	4.34×10^{-20}	mol/(msPa$^{0.5}$)	2697	220	-	[34]
SS316	1.13×10^{-18}	mol/(msPa$^{0.5}$)	7990	290	-	[35]
Inconel 718	1.13×10^{-17}	mol/(msPa$^{0.5}$)	8190	1100	-	[35]
SS403	4.34×10^{-20}	mol/(msPa$^{0.5}$)	7800	310	-	[36]
PP	2.6×10^{-15}	mol/(msPa)	870	-	17.4	[37,38]
HDPE	8.98×10^{-16}	mol/(msPa)	1275	-	27	[39]
CFEP	1.9×10^{-16}	mol/(msPa)	1790	-	4000	[39]
W	4.94×10^{-32}	mol/(msPa$^{0.5}$)	12,750	1045		[40]
Si	1×10^{-8}	mol/(m^{2}sPa$^{0.5}$)	3220	-	-	[41]

Since ensuring the safety of people is very important, it was necessary to assess the risks that are associated with permeation, namely the possibility of explosions. The permeability of H_2 through solid surfaces was studied for the materials of the spheres and of the envelope tank. According to the references [39,42], there are values of permeability with great uncertainties associated, and not always expressed in the same units. In Table 2, Φ represents the permeation value for the conditions at 293.15 K and 101.3 kPa. From this table, it can be concluded that the metal alloys (Al5050-H38, SS403, Inconel 718, W, and SS316) have lower permeation values, although they present higher strength values compared to polymeric materials (PP and HDPE). Composite materials (epoxy fiberglass and CFEP) have higher permeation values and identical or higher strength values compared to metal alloys.

At this juncture, the idea of coupling two materials in the construction of the microsphere came up. Such a combination was tested with two concentric spherical layers, the inner layer to provide the necessary resistance to H_2 permeation and the outer layer to provide structural strength.

Thus, the materials for the microchip, the inner and outer layer, as well as the material that constitutes the envelope tank were chosen according to Table 3.

The Si was chosen for the micro-chip due to its easy tooling [31]; indeed, it is a material widely used in small electronic devices for this reason.

According to Dwivedi et al. [43], materials with high strength, such as steel, steel with a high magnesium content, titanium, and magnesium alloys are prone to embrittlement caused by H_2 when they are under conditions of high temperature, pressure, and exposure time.

Table 3 shows all the studied combinations of materials for each part of the storage system, from the set of materials referred on Table 2.

2.4. Regulations That Must Be Complied: Step 4

The European Regulations on the approval of future hydrogen-powered vehicles is called EU 406/2010 [27]. The standard requirements allow the permeation of metallic container materials to be neglected. However, polymeric materials must be submitted to suitable permeation tests. The research study meets this requirement [30], which concluded that the permeation of polymeric materials is higher than the permeation of metallics materials. At steady state, the maximum allowable permeation flow is 6 Ncm^{3}h^{-1}L^{-1},

being this value per liter of the internal volume of the container and, for safety reasons, it is intended to avoid a possible mixture between H_2 and air in closed spaces, assuming a minimum air renewal per hour of 0.03 [44].

Table 3. Combinations of material for each part of the storage system studied.

Combinations	Lining	Structural Layer	Microchip	Envelope Tank
1	Al 5050-H38	CFEP	Si	Al 5050-H38
2	Al 5050-H38	CFEP	Si	SS316
3	Al 5050-H38	CFEP	Si	SS403
4	Al 5050-H38	CFEP	Si	Inconel 718
5	Al 5050-H38	CFEP	Si	PP
6	Al 5050-H38	CFEP	Si	HDPE
7	SS316	CFEP	Si	Al 5050-H38
8	SS316	CFEP	Si	SS316
9	SS316	CFEP	Si	SS403
10	SS316	CFEP	Si	Inconel 718
11	SS316	CFEP	Si	PP
12	SS316	CFEP	Si	HDPE
13	SS403	CFEP	Si	Al 5050-H38
14	SS403	CFEP	Si	SS316
15	SS403	CFEP	Si	SS403
16	SS403	CFEP	Si	Inconel 718
17	SS403	CFEP	Si	PP
18	SS403	CFEP	Si	HDPE
19	W	CFEP	Si	Al 5050-H38
20	W	CFEP	Si	SS316
21	W	CFEP	Si	SS403
22	W	CFEP	Si	Inconel 718
23	W	CFEP	Si	PP
24	W	CFEP	Si	HDPE
25	PP	CFEP	Si	Al 5050-H38
26	PP	CFEP	Si	SS316
27	PP	CFEP	Si	SS403
28	PP	CFEP	Si	Inconel 718
29	PP	CFEP	Si	PP
30	PP	CFEP	Si	HDPE

Another factor to consider, according to [45], is the temperature, since it affects the permeation of H_2 through the walls. In the current study, it is expected that temperatures during filling (in the case of rapid filling) are approximately 50 °C; however, it is assumed that there may be peaks of 85 °C. In the calculations performed in this study, a correction factor was added, considering that the tests were performed at temperatures below 55 °C [30,46].

The correction factor adopted was 2 [30], since the aging of the material causes an increase in the permeation of H_2, although this phenomenon has not yet been fully understood.

Thus, the value of $C_\%$ must be less than 1% (see Equation (14)), where $C_\%$ represents the volumetric flow of the H_2 ratio that leaves, by permeation, the envelope tank, Q_{H2}, and the sum of the flow of air in space due to air renewal, Qair with Q_{H2}. So,

$$C_\% = \frac{100 \cdot Q_{H2}}{Q_{air} + Q_{H2}}, \tag{14}$$

Qp-H_2, (see Equation (15)), is the maximum allowable flowrate of permeation of H_2, expressed in mL/h/L, i.e., the milliliters of H_2 leaked during one hour per liter of the inner volume of the storage vessel,

$$Q_{p-H_2} = \frac{Q_{air} \cdot C_\%}{100 - C_\%} \cdot \frac{60 \cdot 10^6}{V_{int\,all\,sph} \cdot f_a \cdot f_t} \tag{15}$$

with $V_{int\ all\ sph}$ being the inner volume of the storage vessel (in the present case, the whole set of spheres in the envelope tank), f_a is the aging factor of 2, and f_t is the factor of correction for the temperature; $V_{int\ all\ sph}$ is expressed in liters, Q_{air} and Q_{H2} must be expressed in m^3/min.

In short, the value of permeation varies during the emptying of spheres, either because of the decrease in the pressure within the spheres, or because of temperature or the aging of the spheres. Therefore, the flowrate of H_2 by permeation, across the wall of the sphere, must vary with time.

In the current study, Equations (14) and (15) were used considering the three following scenarios proposed by Adams et al. [30] for domestic garages and parked vehicles; see Table 4.

Table 4. Scenarios for domestic garages and parked vehicles. Adapted from Adams et al. [30].

Features	Scenarios		
	1	2	3
Garage volume (m^3)	50	33	19
Garage free volume (m^3)	46	31	18
Volume of impermeable material (m^3)	4	2	1
Natural ventilation of the garage (ACH)	0.03	0.03	0.03
Natural ventilation of the garage (m^3/h)	1.38	0.93	0.54

2.5. Aim of Calculations: Step 5

In the current study, the value of Q_{H2} of Equation (14) was determined with the procedure described in step 2. Such values were determined over time, for a family vehicle parked inside a common garage for a long period of time; and at the beginning of such parking, the storage system was considered filled with H_2 at the highest pressure. The values of Q_{air} of Equations (14) and (15) were assumed as the air changes flowrates at the garage, taken from Table 4, for the referred three scenarios.

Ultimately, the aim is to see if for the new storage system, the value of $C_\%$, according to Equation (14), is under 1%.

2.6. The Packing Factor (PF): Step 6

The PF indicates the proportion of usable space in the storage system. It must have the highest possible value.

Aigueperse et al. [47] studied the stowage of spheres randomly launched into a container. They concluded that the arrangement of the spheres is identical to the crystalline structures. The simplest combination of spheres is the body-centered cubic structure (BCC), with a packing factor of approximately 0.52.

Other authors also state that the closed hexagonal packing (HCP) [48,49] has the highest PF value, at approximately 0.74.

Regarding the storage of spheres, Dong et al. [50], Silbert et al. [51], and Onoda et al. [52] studied randomly compact packing (PRC) and randomly loose packing (PRL). According to the authors [50], after several studies, the best value achieved for Packing Factor (PF) was 0.64. The authors [51] concluded that PRC is the most efficient arrangement for randomly stowed spheres in a tank, surpassed only by an arrangement obtained through container vibration. Onoda et al. [52], in their experimental tests of glass spheres immersed in a liquid, disregarding the gravitational force, obtained a PF of 0.55.

3. Results and Discussion

All the combinations of materials shown in Table 3 were considered in calculations. The mass of H_2 in each sphere and the envelope tank were calculated along with the time, through Equations (10) and (13), respectively.

The time-step used in all the cases was 5000 s, and during each step, P_{sph} and P_{tank} were assumed constant. Furthermore, on one hand, the time-step was chosen in order

to avoid needless time-consuming calculations because of too small time-steps without a noticeable increase of accuracy in the results, and, on the other hand, to avoid inaccurate results because of too large time-steps. So, the choice of 5000 s as the time-step results from a trade-off between the referred conflicting speed of calculations and accuracy of results but permits the obtaining of reasonably accurate results.

The pressure considered for calculating the permeation of the two layers of spheres was taken as the difference between the pressures within and without the spheres; similarly, the pressure considered for calculating the permeation of the envelope tank was taken as the difference between the pressures within the envelope tank and the atmospheric pressure.

The temperature of the atmosphere and the temperature of the H_2 within either the spheres or the envelope tank were considered to be 293.15 K. The atmospheric pressure was taken as 101,325 Pa. The initial pressure within the spheres was assumed as 71 MPa, whereas the initial pressure in the envelope tank in the space between spheres was taken as 0.5 MPa. The PF was taken as 0.52 because this is the value of PF normally found in the random stackings of spheres.

A first calculation was made to see which combinations of Table 3 correspond to less permeation losses from the spheres into the garage. To do this, a car was parked in a garage with a full H_2 storage system at 700 bar inside the spheres and 5 bar in the space of the envelope tank between spheres. In this situation, the H_2 will naturally permeate through the spheres into the envelope tank and from there, into the garage. The calculation aimed to obtain the time required for reaching 20 bar in the envelope tank between spheres, which obviously should be as long as possible, and at the same time to check if the value of $C_\%$, see Equation (14), at that moment was below 1%, as required by regulations.

To obtain comparable results with those of Adams et al. [30], the storage system was assumed to be installed (i) in large cars, parked in garages with a volume of 50 m^3, with a free volume of 46 m^3 and 0.03 ACH (1.38 m^3/h); (ii) in small cars, parked in garages with a volume of 33 m^3, with a free volume of 31 m^3 and 0.03 ACH (0.93 m^3/h); and (iii) in micro cars, parked in garages with a volume of 19 m^3, with a free volume of 46 m^3 and 0.03 ACH (0.54 m^3/h).

The results are shown in Table 5 and prove that, in all three scenarios, the value of $C_\%$ is well below 1% and that it takes about 2.5 months for the pressure in the envelope tank to rise from 5 to 20 bar, except for the cases of combinations 25 to 30, owing to the material of the lining being PP, whose permeation resistance is very low.

Further analysis was made for combinations 1, 7, and 19 since these combinations correspond to the lowest values of $C_\%$. The evolution of H_2 pressure over time, in spheres and the envelope tank (since the car is parked until the pressure in the envelope tank reaches 20 bar), is shown for combinations 1, 7, and 19, respectively, in Figures 3–5; moreover, the evolution of $C_\%$ over time is shown for combinations 1, 7, and 19, respectively, in Figures 6–8.
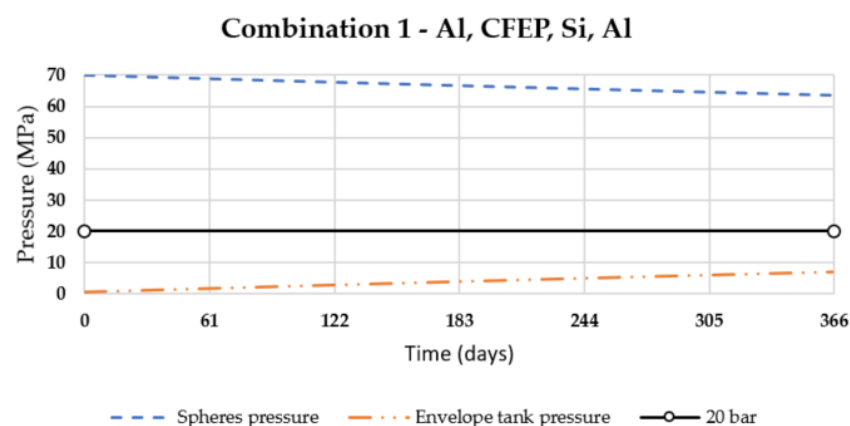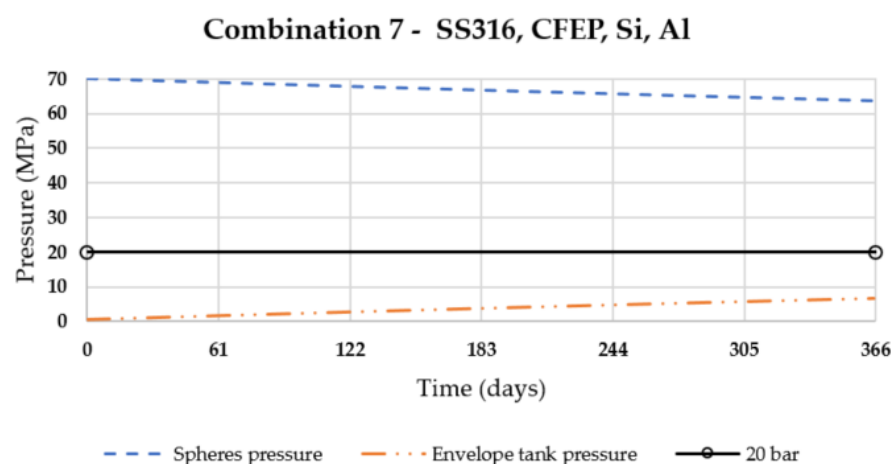

Figure 3. Pressure inside of the spheres and the envelope tank, combination 1 from Table 3.

Table 5. Time to obtain 20 bar in the envelope tank and values of $C_\%$ for the scenarios of Table 4.

Combinations	Elapsed Time (Days)	$C_\% = 100 \times Q_{H2}/(Q_{air} + Q_{H2})$ in Garage Scenarios		
		1	2	3
1	79.6	2.8×10^{-10}	4.1×10^{-10}	7.1×10^{-10}
2	79.6	1.1×10^{-8}	1.6×10^{-8}	2.7×10^{-8}
3	79.6	1.4×10^{-5}	2.1×10^{-5}	3.6×10^{-5}
4	79.6	3.8×10^{-7}	5.6×10^{-7}	9.7×10^{-7}
5	82.6	3.1×10^{-3}	4.7×10^{-3}	8.0×10^{-3}
6	80.4	8.3×10^{-4}	1.2×10^{-3}	2.1×10^{-3}
7	79.6	2.8×10^{-10}	4.1×10^{-10}	7.1×10^{-10}
8	79.6	1.1×10^{-8}	1.6×10^{-8}	2.7×10^{-8}
9	79.6	1.4×10^{-5}	2.1×10^{-5}	3.6×10^{-5}
10	79.6	3.8×10^{-7}	5.6×10^{-7}	9.7×10^{-7}
11	82.6	3.1×10^{-3}	4.7×10^{-3}	8.0×10^{-3}
12	80.4	8.3×10^{-4}	1.2×10^{-3}	2.1×10^{-3}
13	69.4	2.8×10^{-10}	4.1×10^{-10}	7.1×10^{-10}
14	69.4	1.1×10^{-8}	1.6×10^{-8}	2.7×10^{-8}
15	69.4	1.4×10^{-5}	2.1×10^{-5}	3.6×10^{-5}
16	69.4	3.8×10^{-7}	5.6×10^{-7}	9.7×10^{-7}
17	71.8	3.1×10^{-3}	4.7×10^{-3}	8.0×10^{-3}
18	70.0	8.3×10^{-4}	1.2×10^{-3}	2.1×10^{-3}
19	79.6	2.8×10^{-10}	4.1×10^{-10}	7.1×10^{-10}
20	79.6	1.1×10^{-8}	1.6×10^{-8}	2.7×10^{-8}
21	79.6	1.4×10^{-5}	2.1×10^{-5}	3.6×10^{-5}
22	79.6	3.8×10^{-7}	5.6×10^{-7}	9.7×10^{-7}
23	82.6	3.1×10^{-3}	4.7×10^{-3}	8.0×10^{-3}
24	80.4	8.3×10^{-4}	1.2×10^{-3}	2.1×10^{-3}
25	0.8	2.7×10^{-10}	4.0×10^{-10}	6.8×10^{-10}
26	0.8	1.0×10^{-8}	1.5×10^{-8}	2.6×10^{-8}
27	0.8	1.4×10^{-5}	2.0×10^{-5}	3.5×10^{-5}
28	0.8	3.7×10^{-7}	5.4×10^{-7}	9.4×10^{-7}
29	0.8	3.0×10^{-3}	4.5×10^{-3}	7.8×10^{-3}
30	0.8	8.1×10^{-4}	1.2×10^{-3}	2.1×10^{-3}

Figure 4. Pressure inside of the spheres and the envelope tank, combination 7 from Table 3.

Combination 19 - W, CFEP, Si, Al
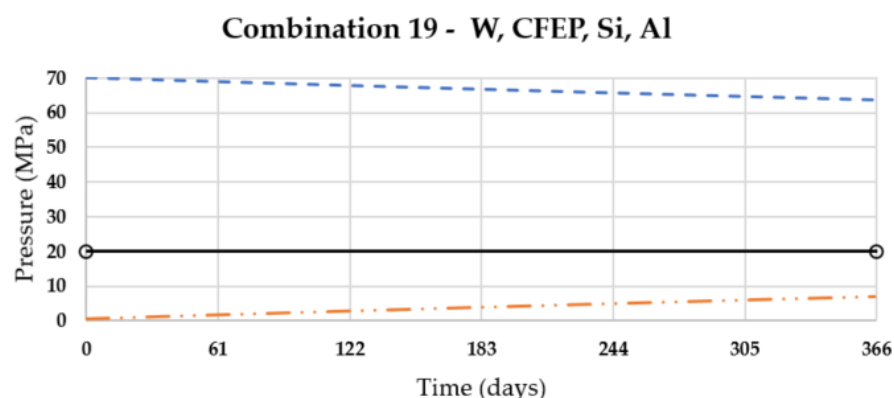
Figure 5. Pressure inside of the spheres and the envelope tank, combination 19 from Table 3.

Combination 1 - Al, CFEP, Si, Al


```
----- Large car    — — Small car    — · — · Micro car
```
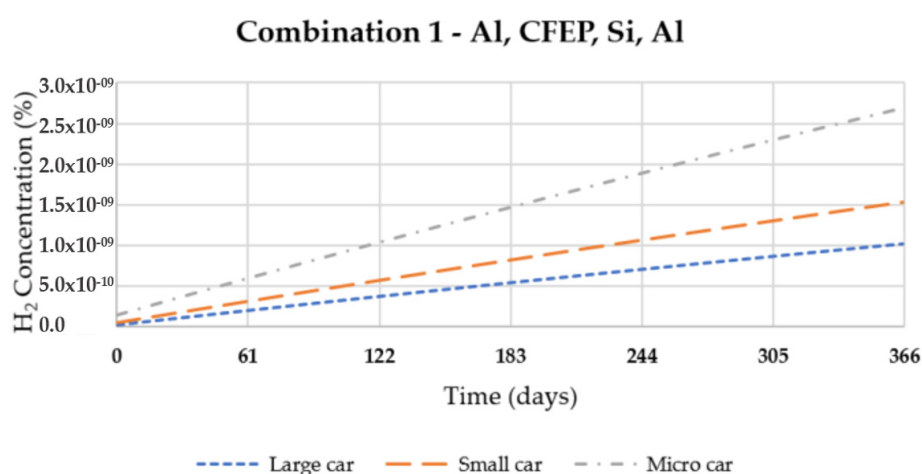
Figure 6. H_2 concentration in the garage, combination 1 from Table 3.

Combination 7 - SS316, CFEP, Si, Al


```
----- Large car    — — Small car    — · — · Micro car
```
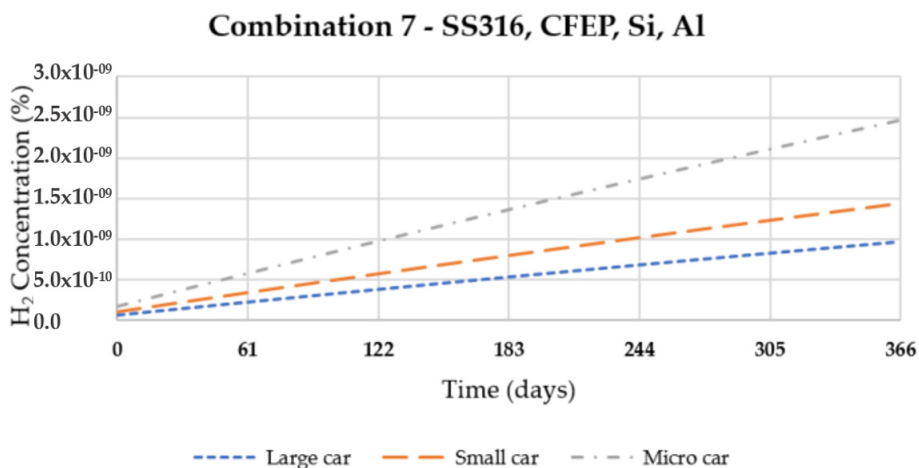
Figure 7. H_2 concentration in the garage, combination 7 from Table 3.

From the graphs of Figures 3–5, it can be seen that as the pressure inside the spheres decreases, the pressure in the envelope tank increases in spite of the permeation from the envelope tank to the garage. This is owing (i) to the fact that the permeation values of the envelope tank are much lower than the permeation values of the spheres and (ii) the pressure in the spheres is much higher than the pressure in the envelope tank.

Graphs of Figures 6–8 show that for all the three scenarios considered, the storage system studied guarantees values of concentration of H_2, even for 1 year of parking, well below the 1% required by European Regulations [27]. Thus, this storage system is safe for the everyday use of hydrogen-propelled cars.
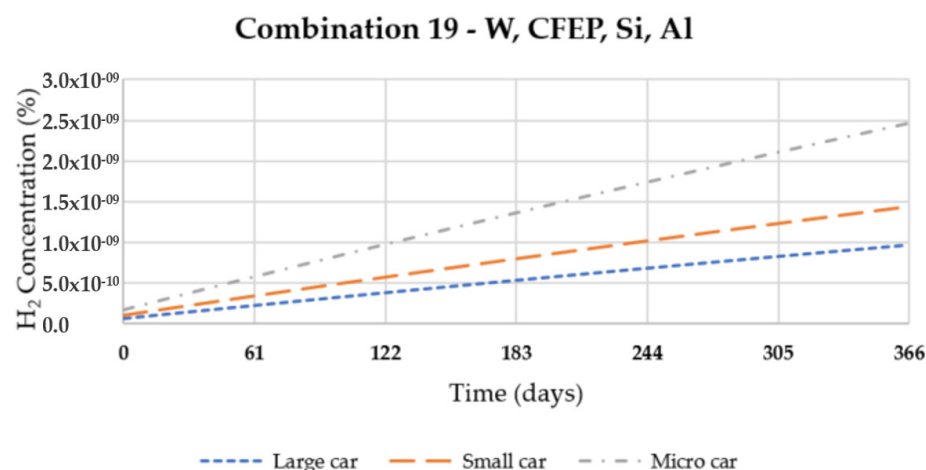
Combination 19 - W, CFEP, Si, Al

Figure 8. H_2 concentration in the garage, combination 19 from Table 3.

4. Conclusions

In this work, the best set of materials for the microchip, sphere, and envelope tank was studied, considering the permeation flowrate.

All the combinations of materials chosen to manufacture the parts of the storage system that exclude the PP allow the safe use of the currently studied storage system. The best option, among the pool of materials chosen, consists of aluminum for the liner of the spheres and the envelope tank, CFEP for the structural layer of the spheres, and Si for the microchip. Moreover, provided that European Regulations are adopted, and following the procedure of Adams et al. [30], if the user of the car leaves it parked in a garage for about 2.5 months, the H_2 storage system never creates a dangerous situation compromising the safety of persons or goods in the vicinity of the car.

Moreover, analytical [53,54] and experimental [54,55] studies over permeation flowrate from containers with CGH_2 provided results of the same order of magnitude obtained from the current study over concentration of H_2 in spaces such as garages.

Anyway, if there is an accident, such as the bursting of spheres, it is most likely that only a few spheres will be involved in it, which, at the outset, minimizes the disastrous consequences of the accident. Therefore, this storage system is intrinsically safer than other storage systems of compressed gaseous H_2.

Naturally, some of the results presented in this paper can be slightly corrected in the future, when more accurate values of permeation for materials are available. In any case, it is not likely that such corrections will entail conclusions that may fundamentally contradict the present ones.

Abbreviations

List of Symbols

A	Area
ACH	Air changes per hour
C	Ratio of flowrate of H_2 and flowrate of H_2 and air
D	Diffusivity
fa	Aging factor
ft	Correction factor for the temperature
GED	Gravimetric energy density
LHV	Low heating value
M	Mass
MW	Molecular weight
$\dot{n}$	Permeation mole flowrate
N	Number of spheres
P	Pressure
PF	Packing Factor
Q	Flowrate
r	Radius
R	Gas constant, resistance to diffusion
S	Solubility
T	Temperature
t	Time
V	Volume
VED	Volumetric energy density
x	Mole fraction
Z	Compressibility factor

Subscripts

i	inner
int all sph	Inside all spheres
in sph	Inside the sphere
int tank	Inside the tank
o	outer
p-H_2	Maximum H_2 allowable permeation
sph	Sphere
ult	ultimate
u	universal
yield	Yield

Greek Symbols

Δ	Variation
ρ	Density
σ	Stress
Φ	Permeation coefficient

References

1. World Bank—Fossil Fuel Energy Consumption Data, Energy Foss Fuels Consum. 2016. Available online: http://data.worldbank.org/indicator/EG.USE.COMM.FO.ZS (accessed on 20 September 2021).
2. Strauss, M. EU to Boost Green Hydrogen Use for Decarbonisation, Focus on Energy Efficiency, Reuters. Available online: https://www.reuters.com/article/us-climate-change-eu-hydrogen/eu-to-boost-green-hydrogen-use-for-decarbonisationfocus-on-energy-efficiency-idUSKBN2491JA (accessed on 15 February 2021).
3. European Council of the European Union. Available online: https://www.consilium.europa.eu/en/press/press-releases/2020/12/18/paris-agreement-council-transmits-ndc-submission-on-behalf-of-eu-and-member-states/ (accessed on 11 February 2021).
4. Herrero, S.T.; Nicholls, L.; Strengers, Y. Smart home technologies in everyday life: Do they address key energy challenges in households? *Curr. Opin. Env. Sustain.* **2018**, *31*, 65–70. [CrossRef]
5. Spiegel, C. *Designing and Building Fuel Cells*, 1st ed.; McGraw-Hill: New York, NY, USA, 2007; ISBN -13: 978-0-07-148977-5.
6. Zhang, F.; Zhao, P.; Niu, M.; Maddy, J. The survey of key technologies in hydrogen energy storage. *Int. J. Hydrog. Energy* **2016**, *41*, 14535–14552. [CrossRef]

7. Acar, C.; Bicer, Y.; Demir, M.E.; Dincer, I. Transition to a new era with light-based hydrogen production for a carbon-free society: An overview. *Int. J. Hydrog. Energy* **2019**, *44*, 25347–25364. [CrossRef]

8. Dincer, I.; Acar, C. Smart energy solutions with hydrogen options. *Int. J. Hydrog. Energy* **2018**, *43*, 8579–8599. [CrossRef]

9. Nastasi, B.; Lo Basso, G. Hydrogen to link heat and electricity in the transition towards future Smart Energy Systems. *Energy* **2016**, *110*, 5–22. [CrossRef]

10. Europe Hydrogen Refuelling Infrastructure. Available online: https://h2me.eu/about/hydrogen-refuelling-infrastructure/ (accessed on 15 February 2021).

11. USA Hydrogen Refuelling Infrastructure. Available online: https://afdc.energy.gov/fuels/hydrogen_locations.html#/find/nearest?fuel=HY (accessed on 11 February 2021).

12. O´Hayre, R.; Cha, S.; Colella, W.; Prinz, F. *Fuel Cell Fundamentals*, 1st ed.; John Wiley & Sons: New York, NY, USA, 2006; ISBN: 978-0471741480.

13. Acar, C.; Bicer, Y. Review and evaluation of hydrogen production options for better environment. *J. Clean. Prod.* **2019**, *218*, 835–849. [CrossRef]

14. Handwerker, M.; Wellnitz, J.; Marzbani, H. Comparison of Hydrogen Powertrains with the Battery Powered Electric Vehicle and Investigation of Small-Scale Local Hydrogen Production Using Renewable Energy. *Hydrogen* **2021**, *2*, 76–100. [CrossRef]

15. Sunliang, C. Comparison of the energy and environmental impact by integrating a H_2 vehicle and an electric vehicle into a zero-energy building. *Energy Convers. Manag.* **2016**, *123*, 153–173.

16. Koroma, M.; Brown, N.; Cardellini, G.; Messagie, M. Prospective Environmental Impacts of Passenger Cars under Different Energy and Steel Production Scenarios. *Energies* **2020**, *13*, 6236. [CrossRef]

17. Lys, A.; Fadonougbo, J.; Faisal, M.; Suh, J.; Lee, Y.; Shim, J.; Park, J.; Cho, Y. Enhancing the Hydrogen Storage Properties of AxBy Intermetallic Compounds by Partial Substitution: A Short Review. *Hydrogen* **2020**, *1*, 38–63. [CrossRef]

18. Fonseca, J.D.; Camargo, M.; Commenge, J.-M.; Falk, L.; Gil, I.D. Trends in design of distributed energy systems using hydrogen as energy vector: A systematic literature review. *Int. J. Hydrog. Energy* **2018**, *44*, 9486–9504. [CrossRef]

19. Tarkowski, R. Underground hydrogen storage: Characteristics and prospects. *Renew. Sustain. Energy Rev.* **2019**, *105*, 86–94. [CrossRef]

20. Wei, Q.; Zhang, X.; Oh, B. The effect of driving cycles and H_2 production pathways on the lifecycle analysis of hydrogen fuel cell vehicle: A case study in South Korea. *Int. J. Hydrog. Energy* **2021**, *46*, 7622–7633. [CrossRef]

21. Bethoux, O. Hydrogen Fuel Cell Road Vehicles: State of the Art and Perspectives. *Energies* **2020**, *13*, 5843. [CrossRef]

22. Bethoux, O. Hydrogen Fuel Cell Road Vehicles and Their Infrastructure: An Option towards an Environmentally Friendly Energy Transition. *Energies* **2020**, *13*, 6132. [CrossRef]

23. Sapre, S.; Pareek, K.; Rohan, R.; Singh, P. H_2 refueling assessment of composite storage tank for fuel cell vehicle. *Int. J. Hydrog. Energy* **2019**, *44*, 23699–23707. [CrossRef]

24. Larminie, J.; Dicks, A. *Fuel Cell Systems Explained*, 2nd ed.; John Wiley & Sons, Ltd: West Sussex, UK, 2003; ISBN: 978-0-470-84857-9.

25. Baptista, A.; Pinho, C.; Pinto, G.; Ribeiro, L.; Monteiro, J.; Santos, T. Assessment of an Innovative Way to Store Hydrogen in Vehicles. *Energies* **2019**, *12*, 1762. [CrossRef]

26. Stenmark, L. *Hydrogen Effects on Silicon Microsystems*; (Uppsala University, Sweden). High Pressure Hydrogen Storage. 2009. Available online: https://apps.dtic.mil/sti/citations/ADA504550 (accessed on 3 July 2021).

27. European Union. Commission Regulation (EU) No 406/2010 of 26 April 2010 implementing Regulation (EC) No 79/2009 of the European Parliament and of the Council on type-approval of hydrogen-powered motor vehicle. *Off. J. Eur. Union* **2010**, *53*, L122/1–L122/107.

28. Kim, Y.S.; Kim, S.S.; Choe, B.H. The Role of Hydrogen in Hydrogen Embrittlement of Metals: The Case of Stainless Steel. *Metals* **2019**, *9*, 406. [CrossRef]

29. Fu, L.; Fang, H. Formation Criterion of Hydrogen-Induced Cracking in Steel Based on Fracture Mechanics. *Metals* **2018**, *8*, 940. [CrossRef]

30. Adams, P.; Bengaouer, A.; Cariteau, B.; Molkov, V.; Venetsanos, A. Allowable hydrogen permeation rate from road vehicles. *Int. J. Hydrog. Energy* **2011**, *36*, 2742–2749. [CrossRef]

31. Crowl, A.; Jo, Y. The hazards and risks of hydrogen. *J. Loss Prev. Process. Ind.* **2007**, *20*, 158–164. [CrossRef]

32. Barth, R.R.; Simmons, K.L.; San Marchi, C. *Polymers for Hydrogen Infrastructure and Vehicle Fuel Systems*; In Sandia National Laboratories: Livermore, CA, USA, 2013.

33. Perry, R.H.; Green, D.W.; Maloney, J.O. *Perry's Chemical Engineers' Handbook*, 7th ed.; McGraw-Hill: New York, NY, USA, 1997; ISBN 0-07-049841-5.

34. Song, W.; Du, J.; Xu, Y.; Long, B. A study of hydrogen permeation in aluminum alloy treated by various oxidation processes. *J. Nucl. Mater.* **1997**, *246*, 139–143. [CrossRef]

35. Van Deventer, E.H.; Maroni, V.A. Hydrogen permeation characteristics of some austenitic and nickel-base alloys. *J. Nucl. Mater.* **1980**, *92*, 103–111. [CrossRef]

36. Schefer, R.W.; Hout, W.G.; San Marchi, C.; Chernicoff, W.P.; Englom, L. Characterization of leaks from compressed hydrogen dispensing systems and related components. *Int. J. Hydrog. Energy* **2006**, *31*, 1247–1260. [CrossRef]

37. Paiva, L.B.; Morales, A.R.; Guimarães, T.R. Propriedades mecânicas de nanocompósitos de polipropileno e montmorilonita organofílica. *Polímeros* **2006**, *16*, 2. [CrossRef]

38. Paul, D.R. Reformulation of the solution-diffusion theory of reverse osmosis. *J. Membr. Sci.* **2004**, *241*, 371–386. [CrossRef]
39. Humpenoder, J. Gas permeation of fibre reinforced plastics. *Cryogenics* **1998**, *38*, 143–147. [CrossRef]
40. Steward, S.A. *Review of Hydrogen Isotope Permeability Through Materials*; Lawrence Livermore National Laboratory: Berkeley, CA, USA, 1983.
41. Suda, H.; Yamauchi, H.; Uchimaru, Y.; Fujiwara, I.; Haraya, K. Preparation and gas permeation properties of silicon carbidebased inorganic membranes for hydrogen separation. *Desalination* **2006**, *193*, 252–255. [CrossRef]
42. Schultheiß, D. Permeation Barrier for Lightweight Liquid Hydrogen Tanks. Ph.D. Thesis, University at Augsburg, Augsburg, Germany, 16 April 2007.
43. Dwivedi, S.K.; Vishwakarma, M. Hydrogen embrittlement in different materials: A review. *Int. J. Hydrog. Energy* **2018**, *43*, 21603–21616. [CrossRef]
44. Waterland, L.R.; Powars, C.; Stickes, P. *Safety Evaluation of the FuelMaker Home Refueling Concept Final Report*; National Renewable Energy Laboratory: Golden, CO, USA, 2005.
45. Mitlitsky, F.; Weisberg, H.A.; Myers, B. *Vehicular Hydrogen Storage Using Lightweight Tanks*; Lawrence Livermore National Laboratory: Berkeley, CA, USA, 2000.
46. Moretto, P.; Acosta-Iborra, B.; Baraldi, D.; Galassi, M.; De Miguel, N.; Ortiz Cebolla, R. *Onboard Compressed Hydrogen Storage: Fast Filling*; IA HySafe and JRC IET Workshop, Research Priorities and Knowledge Gaps in Hydrogen Safety: Berlin, Germany, 2012; pp. 1–15.
47. Aigueperse, J.; Mollar, P.; Devilliers, D.; Chemla, M.; Faron, R.; Romano, R.; Cuer, J. Fluorine Compounds, Inorganic. In *Ullmann's Encyclopedia of Industrial Chemistry*; Wiley: Hoboken, NJ, USA, 2012; Volume 15.
48. Hales, T.; Ferguson, S. A Formulation of the Kepler Conjecture. *Discret. Comput. Geom.* **2006**, *36*, 21–69. [CrossRef]
49. Hales, T.; Adams, M.; Bauer, G.; Dang, T.; Harrison, J.; Hoang, L.; Zumkeller, R. A Formal Proof of the Kepler Conjecture. *Forum Math.* **2017**, *5*, 1–29. [CrossRef]
50. Dong, K.; Yang, R.; Zou, R.; Yu, A. Role of Interparticle Forces in the Formation of Random Loose Packing. *Phys. Rev. Lett.* **2006**, *96*, 145505-1–145505-4. [CrossRef]
51. Silbert, L. Jamming of frictional spheres and random loose packing. *Soft Matter* **2010**, *13*, 2918–2924. [CrossRef]
52. Onoda, G.; Liniger, E. Random Loose Packings of Uniform Spheres and the Dilatancy Onset. *Phys. Rev. Lett.* **1990**, *64*, 2727–2730. [CrossRef]
53. Saffers, J.B.; Makarov, D.; Molkov, V.V. Modelling and numerical simulation of permeated hydrogen dispersion in a garage with adiabatic walls and still air. *Int. J. Hydrog. Energy* **2011**, *36*, 2582–2588. [CrossRef]
54. Venetsanos, A.G.; Papanikolaou, E.; Cariteau, B.; Adams, P.; Bengaouer, A. Hydrogen permeation from CGH2 vehicles in garages: CFD dispersion calculations and experimental validation. *Int. J. Hydrog. Energy* **2010**, *35*, 3848–3856. [CrossRef]
55. Gentilhomme, O.; Proust, C.; Jamois, D.; Tkatschenko, I.; Cariteau, B.; Studer, E.; Masset, F.; Joncquet, G.; Amielh, M.; Anselmet, F. Data for the evaluation of hydrogen risks onboard vehicles: Outcomes from the French project drive. *Int. J. Hydrog. Energy* **2012**, *37*, 17645–17654. [CrossRef]